Empirical mode decomposition for seismic time-frequency analysis

Jiajun Han[1] and Mirko van der Baan[1]

ABSTRACT

Time-frequency analysis plays a significant role in seismic data processing and interpretation. Complete ensemble empirical mode decomposition decomposes a seismic signal into a sum of oscillatory components, with guaranteed positive and smoothly varying instantaneous frequencies. Analysis on synthetic and real data demonstrates that this method promises higher spectral-spatial resolution than the short-time Fourier transform or wavelet transform. Application on field data thus offers the potential of highlighting subtle geologic structures that might otherwise escape unnoticed.

INTRODUCTION

The most common tool for spectral analysis is the Fourier transform; however, if applied to the entire trace, it provides no information about local frequency variations. Such knowledge of how the frequency content of a signal varies in time can be significant. Local time-frequency analysis is commonly used in seismic processing and interpretation, and there is therefore a rich history and diversity in developed decomposition methodologies.

Taner et al. (1979) propose the instantaneous frequency attribute which is useful in correlation and appears to indicate hydrocarbon accumulations. The wavelet transform developed by Morlet et al. (1982) manifests more flexibility and superiority in geophysical applications (Chakraborty and Okaya, 1995). Partyka et al. (1999) first demonstrated the value of spectral decomposition in 3D seismic data interpretation using tapered short-time Fourier transforms. Taner et al. (1979) and Barnes (2000) improve the interpretability of instantaneous attributes by using a weighted average window. Castagna et al. (2003) demonstrate the suitability of the instantaneous spectrum for hydrocarbon detection. Liu and Marfurt (2007) also use the instantaneous spectrum for detecting geologic structures. Odebeatu et al. (2006) apply the S-transform

to reflection data and relate the gas saturation to a clear spectral signature. Li and Zheng (2008) employ the Wigner-Ville distribution for carbonate reservoir characterization. Reine et al. (2009) find transforms with varying time windows (e.g., wavelet transform and S-transform) allow for more robust estimation of seismic attenuation. Most recently, local attributes derived from an inversion-based time-frequency analysis have also been used in seismic interpretation (Liu et al., 2011).

Time-frequency decomposition maps a 1D signal of time into a 2D image of frequency and time, which describes how the frequency content varies with time. The widely used short-time Fourier transform calculates the fast discrete Fourier transform in each time window to compute the spectrogram. The window length determines the tradeoff between time and frequency resolution as the decomposition basis of sine and cosine waves can only provide a fixed spectral resolution (Mallat, 2008). To overcome the limitations of the short-time Fourier transform, wavelet-based methods have been applied for seismic time-frequency analysis. Chakraborty and Okaya (1995) compare the wavelet transform with Fourier-based methods for performing time-frequency analysis on seismic data, and show the superiority of the wavelet transform in terms of spectral resolution. Likewise, the S-transform is proposed by Stockwell et al. (1996). It can be interpreted as a hybrid of the wavelet transform and short-time Fourier transform. Short-time Fourier, wavelet, and S-transforms have all been successfully applied to seismic time-frequency analysis; and yet, they are all inherently limited in terms of time-frequency resolution by their intrinsic choice of decomposition basis. The computation of instantaneous frequencies seems to offer the highest possible time-frequency resolution as an individual frequency is obtained at each time sample. Unfortunately, negative frequencies, which hold uncertain physical interpretation, are not uncommon (Barnes, 2007; Fomel, 2007). In this paper, we explore the possibilities of using the empirical mode decomposition (EMD) (Huang et al., 1998) in combination with instantaneous frequencies, because this is guaranteed to produce positive values only.

The empirical mode decomposition method developed by Huang et al. (1998) is a powerful signal analysis technique for

---

nonstationary and nonlinear systems. EMD decomposes a seismic signal into a sum of intrinsic oscillatory components, called "intrinsic mode functions" (IMFs). Each IMF has different frequency components, potentially highlighting different geologic and stratigraphic information. Furthermore, high-resolution time-frequency analysis is possible by combining EMD with the instantaneous frequency. The resulting time-frequency resolution promises to be significantly higher than that obtained using traditional time-frequency analysis tools, such as short-time Fourier and wavelet transforms.

The empirical mode decomposition methods have progressed from EMD to ensemble empirical mode decomposition (EEMD) (Wu and Huang, 2009), and a complete ensemble empirical mode decomposition (CEEMD) has recently been proposed by Torres et al. (2011). Even though EMD methods offer many promising features for analyzing and processing geophysical data, there have been few applications in geophysics. Magrin-Chagnolleau and Baraniuk (1999) and Han and Van der Baan (2011) use EMD to obtain robust seismic attributes. Battista et al. (2007) exploit EMD to remove cable strum noise in seismic data. Bekara and Van der Baan (2009) eliminate the first EMD component in the f-x domain to attenuate random and coherent seismic noise. Huang and Milkereit (2009) use the EEMD to analyze the time-frequency distribution of well logs.

The objective of this paper is to show the suitability of EMD-based methods for seismic time-frequency analysis. First, we describe and illustrate the various EMD procedures. Next, using a synthetic example, we show the combination of CEEMD with instantaneous frequencies promises higher time-frequency resolution than the short-time Fourier or wavelet transforms. Finally, we apply the technique on field data to highlight various geologic structures.

THEORY

Empirical mode decomposition

EMD decomposes a data series into a finite set of signals, called IMFs. The IMFs represent the different oscillations embedded in the data. They satisfy two conditions: (1) in the whole data set, the number of extrema, and the number of zero crossings must either equal or differ by one at most; and (2) at any point, the mean value of the envelope defined by the local maxima and the envelope defined by the local minimums is zero. These conditions are necessary to ensure that each IMF has a localized frequency content by preventing frequency spreading due to asymmetric waveforms (Huang et al., 1998).

EMD is a fully data-driven separation of a signal into fast and slow oscillation components. The IMFs are computed recursively, starting with the most oscillatory one. The decomposition method uses the envelopes defined by the local maxima and the local minimums of the data series. Once the maxima of the original signal are identified, cubic splines are used to interpolate all the local maxima and construct the upper envelope. The same procedure is used for local minimums to obtain the lower envelope. Next, one calculates the average of the upper and lower envelopes and subtracts it from the initial signal. This interpolation process is continued on the remainder. This sifting process terminates when the mean envelope is reasonably zero everywhere, and the resultant signal is designated as the first IMF. The first IMF is subtracted from the data and the difference is treated as a new signal on which the same sifting procedure is applied to obtain the next IMF. The decomposition is stopped when the last IMF has a small amplitude or becomes monotonic (Huang et al., 1998; Bekara and van der Baan, 2009; Han and van der Baan, 2011). The sifting procedure ensures the first IMFs contain the detailed components of the input signal; the last one solely describes the signal trend.

Some properties that render EMD interesting for seismic signal analysis are (1) the decomposition is complete in the sense that summing all IMFs reconstructs the original input signal and no loss of information is incurred; (2) IMFs are quasiorthogonal such that the crosscorrelation coefficients between the different IMFs are always close to zero; (3) the IMFs have partially overlapping frequency contents differentiating the decomposition from simple bandpass filters; (4) no predefined decomposition basis is defined in contrast with Fourier, wavelet, and S-transforms (Huang et al., 1998; Flandrin et al., 2004; Bekara and Van der Baan, 2009).

Unfortunately, as desirable as the last two properties can be, they may also constitute a major obstacle restricting the performance of EMD due to intermittency and mode mixing (Huang, 1999; Huang et al., 2003). Mode mixing is defined as a single IMF consisting of signals of widely disparate scales or a signal of a similar scale residing in different IMF components (Huang and Wu, 2008). Deering and Kaiser (2005) try to use signal masking to solve the mode mixing problem. However, the masking function is complicated to estimate in real-world applications. In the next section, we therefore introduce the recently proposed ensemble and complete ensemble EMD variants designed to prevent mode mixing.

Ensemble empirical mode decomposition

Based on the filter bank structure of EMD (Flandrin et al., 2004), Wu and Huang (2009) propose the ensemble EMD to overcome mode mixing. EEMD is a noise-assisted analysis method. It injects noise into the decomposition algorithm to stabilize its performance.

The implementation procedure for EEMD is simple (Wu and Huang, 2009):

1) Add a fixed percentage of Gaussian white noise onto the target signal.
2) Decompose the resulting signal into IMFs.
3) Repeat steps (1) and (2) several times, using different noise realizations.
4) Obtain the ensemble averages of the corresponding individual IMFs as the final result.

The added Gaussian white noise series are zero mean with a constant flat-frequency spectrum. Their contribution thus cancels out and does not introduce signal components not already present in the original data. The ensemble-averaged IMFs maintain therefore their natural dyadic properties and effectively reduce the chance of mode mixing.

Although EEMD can improve EMD performance, it does leave another question: Is it a complete decomposition? Does the sum of all resulting IMFs reconstruct the original signal exactly? Unfortunately, by design, each individual noise-injected EMD application can produce a different number of IMFs. Summing the ensemble-averaged IMFs does not perfectly recreate the original signal, although the reconstruction error decreases with increasing number of employed noise realizations at the expense of increasing computation times.

Complete ensemble empirical mode decomposition

Complete ensemble empirical mode decomposition is also a noise-assisted method. The procedure of CEEMD can be described as follows (Torres et al., 2011):

First, add a fixed percentage of Gaussian white noise onto the target signal, and obtain the first EMD component of the data with noise. Repeat the decomposition I times using different noise realizations and compute the ensemble average to define it as the first IMF_1 of the target signal. Thus,

$$\mathrm{IMF}_1 = \frac{1}{I}\sum_{i=1}^{I} E_1[x + \epsilon w_i], \tag{1}$$

where IMF_1 is the first EMD component of the target signal x, w_i is zero-mean Gaussian white noise with unit variance, ϵ is a fixed coefficient, $E_i[\ ]$ produces the ith IMF component and I is the number of realizations.

Then calculate the first signal residue r_1,

$$r_1 = x - \mathrm{IMF}_1. \tag{2}$$

Next, decompose realizations $r_1 + \epsilon E_1[w_i]$, $i = 1, 2, \ldots, I$, until they reach their first IMF conditions and define the ensemble average as the second IMF_2

$$\mathrm{IMF}_2 = \frac{1}{I}\sum_{i=1}^{I} E_1[r_1 + \epsilon E_1[w_i]]. \tag{3}$$

For $k = 2, 3, \ldots, K$, calculate the kth residue: $r_k = r_{(k-1)} - \mathrm{IMF}_k$, then extract the first IMF component of $r_k + \epsilon E_k[w_i]$, $i = 1, 2, \ldots, I$ and compute again their ensemble average to obtain $\mathrm{IMF}_{(k+1)}$ of the target signal

$$\mathrm{IMF}_{(k+1)} = \frac{1}{I}\sum_{i=1}^{I} E_1[r_k + \epsilon E_k[w_i]]. \tag{4}$$

The sifting process is continued until the last residue does not have more than two extrema, producing

$$R = x - \sum_{k=1}^{K} \mathrm{IMF}_k, \tag{5}$$

where R is the final residual, and K is the total number of IMFs. Therefore the target signal can then be expressed as

$$x = \sum_{k=1}^{K} \mathrm{IMF}_k + R. \tag{6}$$

Equation 6 makes CEEMD a complete decomposition method (Torres et al., 2011). Compared with EMD and EEMD, CEEMD not only solves the mode mixing predicament, but also provides an exact reconstruction of the original signal. Therefore, it is more suitable than EMD or EEMD to analyze seismic signals.

Instantaneous frequency

The local symmetry property of the IMFs ensures that instantaneous frequencies are always positive, thereby rendering EMD or its variants interesting for time-frequency analysis (Huang et al., 1998). Seismic instantaneous attributes (Taner et al., 1979) are derived from the seismic trace $x(t)$ and its Hilbert transform $y(t)$ by computing its analytic signal, given by

$$z(t) = x(t) + iy(t) = R(t)\exp[i\theta(t)], \tag{7}$$

where $R(t)$ and $\theta(t)$ denote the instantaneous amplitude and instantaneous phase, respectively. Instantaneous amplitude is the trace envelope, also called reflection strength, defined as,

$$R(t) = \sqrt{x^2(t) + y^2(t)}. \tag{8}$$

Instantaneous frequency $f(t)$ is defined as the first derivative of instantaneous phase. Thus,

$$f(t) = \frac{1}{2\pi}\frac{d\theta(t)}{dt}. \tag{9}$$

To prevent ambiguities due to phase unwrapping in equation 9, the instantaneous frequency can be calculated instead from

$$f(t) = \frac{1}{2\pi}\frac{x(t)y'(t) - x'(t)y(t)}{x^2(t) + y^2(t)}, \tag{10}$$

where prime denotes derivative with respect to time.

We use equations 8 and 10 to compute instantaneous amplitudes and frequencies for each IMF. Contrary to classical application of instantaneous attributes to the original signal, this procedure produces a multitude of instantaneous frequencies at each time sample, namely one for each IMF, allowing for a more in-depth signal analysis. The result is a time-frequency distribution that is uniformly sampled in time but not in frequency, contrary to, for instance, the short-time Fourier transform. There are as many instantaneous frequencies as IMFs, but most applications produce up to a dozen IMFs, creating very sparse time-frequency representations.

We also compute the peak frequency of the various IMFs and other decomposition methods to create a single attribute. It is defined as the frequency where the maximum energy in each time sample occurs. Peak frequency extraction is a useful kind of spectral decomposition technique which has been widely applied in signal processing research (Marfurt and Kirlin, 2001; Boashash and Mesbah, 2004).

This attribute has the advantage that it produces a single image convenient for interpretation purposes. Further analysis using the individual frequency slices remains always feasible. In a similar fashion, Marfurt and Kirlin (2001) introduce a mean-frequency attribute as a way to summarize the information contained in a spectral decomposition.

EXAMPLES

Synthetic data: EMD, EEMD, and CEEMD

In this section, we first compare the various EMD-based methods using synthetic signals to demonstrate the advantages of CEEMD. We then show that instantaneous spectral analysis after CEEMD has higher time-frequency resolution than traditional tools, like the short-time Fourier and wavelet transforms.

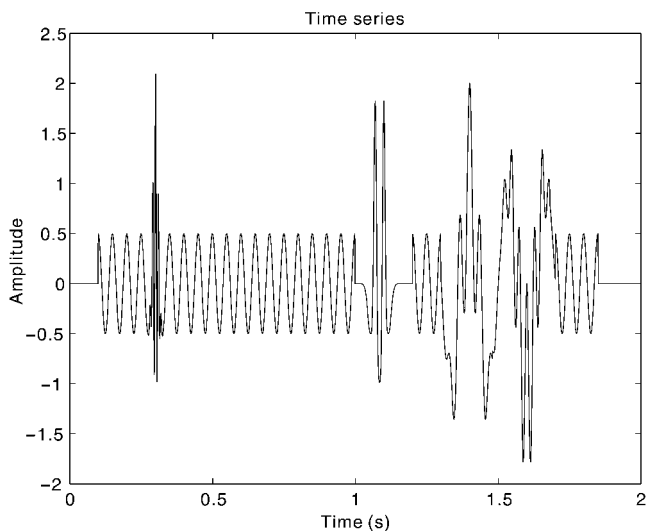The signal in Figure 1 is comprised of an initial 20 Hz cosine wave, superposed 100 Hz Morlet atom at 0.3 s, two 30 Hz Ricker

wavelets at 1.07 and 1.1 s, and three different frequency components between 1.3 and 1.7 s of, respectively, 7, 30, and 40 Hz. Note that the 7 Hz frequency components are not continuous, and comprise less than one-period portions, appearing at 1.37, 1.51, and 1.65 s.

EMD decomposes the synthetic data into seven IMFs (Figure 2). The IMFs in Figure 2 show mode-mixing deficiencies. IMF1 does not solely extract the high-frequency Morlet atom, but is polluted with low-frequency components. Likewise, IMF2 and IMF3 mix low- and high-frequency components from a variety of signal components. This makes it difficult to recognize the individual contributions of each component to various IMFs, thereby complicating signal analysis.

Figure 1. Synthetic example: background 20 Hz cosine wave, superposed 100 Hz Morlet atom at 0.3 s, two 30 Hz Ricker wavelets at 1.07 and 1.1 s, and there are three different frequency components between 1.3 and 1.7 s.
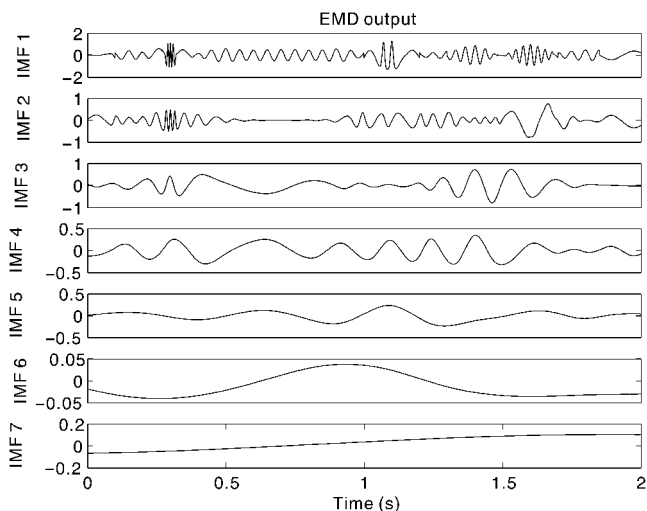
Figure 2. EMD output displaying mode mixing. IMF1 extracts the high-frequency Morlet atom and some low-frequency components. IMF2 and IMF3 also mix different signal components.

Figure 3 contains the EEMD output with 10% added Gaussian white noise and 100 realizations. The mode-mixing problem is reduced, to a large extent; for instance, the 100 Hz Morlet atom is completely retrieved in IMF1. IMF2 mainly contains the 40 Hz signal, which is the second highest frequency component. Some slight mode mixing still occurs in IMF3 and IMF4, but at a significantly reduced level compared with the EMD output.

The CEEMD result also using 10% Gaussian white noise and 100 realizations is shown in Figure 4. The resulting IMF1 is similar to the one obtained by EEMD, retrieving the 100 Hz Morlet atom completely. The resulting IMF2 and IMF3 contain mostly the 40 Hz signal at 1.6 s as well as some other higher frequency components, and IMF4 reflects the two 30 Hz Ricker wavelets around 1.1 s, 30 Hz frequency component at 1.4 s, and the remainder of the 40 Hz signal at 1.6 s. The background 20 Hz cosine wave is mainly reflected in IMF5. CEEMD is least affected by mode mixing of all EMD variants.

Figure 5 displays the reconstruction error for EEMD and CEEMD results. EEMD does not perfectly reproduce the original signal with a reconstruction error of about 0.5% of the total energy; the CEEMD one is close to machine precision and thus negligible.

Synthetic data: Instantaneous frequencies

After the CEEMD decomposition, each IMF is locally symmetric, such that the instantaneous frequency of each IMF is smoothly varying and guaranteed to be positive. We compute the instantaneous frequency of each IMF using equation 10 and
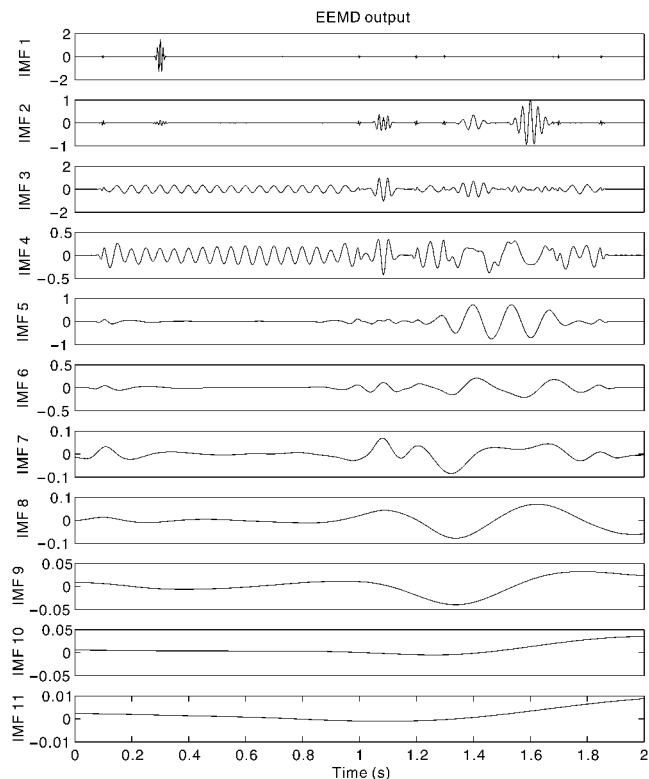

Figure 3. EEMD output with 10% added Gaussian white noise and 100 realizations. Although some mode mixing still occurs in IMF3 and IMF4, the mode mixing problem is reduced to a large extent compared with the EMD output (Figure 2).

associated instantaneous amplitude with equation 8. It is possible to smooth the resulting time-frequency image by means of a convolution with a 2D Gaussian filter of prespecified width. This is useful for display purposes and initial comparison with other time-frequency transforms. Next, we compare the resulting instantaneous spectrum with the short-time Fourier and wavelet transforms for the same synthetic trace shown in Figure 1.

All three methods can discriminate the various frequency components between 1.2 and 2 s, namely the 7, 30, and 40 Hz signals, with acceptable temporal and spectral resolution. None of these three methods can identify the individual portions of the three 7 Hz frequency components, but solely their joint presence. The short-time Fourier transform with a 170 ms time window (Figure 6) does not distinguish between the two Ricker wavelets clearly at 1.07 and 1.1 s due to its fixed time-frequency resolution and their close spacing of 30 ms. Wavelet analysis (Figure 7) fares better; however, the spectral resolution for the 100 Hz Morlet wavelet at 0.3 s is poor.

Figure 8 displays the instantaneous spectrum after CEEMD. The 100 Hz Morlet wavelet, both 30 Hz Ricker wavelets, and three different frequency components are recovered with the highest time-frequency resolution. A small Gaussian weighted filter with width of 6×6 time and frequency samples is applied to the instantaneous spectrum for display purposes.

After calculating the instantaneous frequency, we can control the time-frequency resolution by varying the size of Gaussian weighted filter. Figure 9 shows the resulting instantaneous spectrum using a 30×30 Gaussian-weighted filter, creating a result more comparable to the short-time Fourier and wavelet transforms (Figures 6 and 7).

This synthetic example shows the potentially significantly higher time-frequency resolution of CEEMD combined with instantaneous frequencies over that obtainable with the short-time Fourier and wavelet transforms.

Real data

We next apply the various time-frequency analysis tools on a seismic data set from a sedimentary basin in Canada. There are Cretaceous meandering channels at 0.42 s between common-midpoints (CMPs) 75 and 105 and CMPs 160 and 180, respectively.

Figure 5. Reconstruction error for EEMD and CEEMD results. EEMD can lead to nonnegligible reconstruction error, whereas it is close to machine precision for CEEMD.
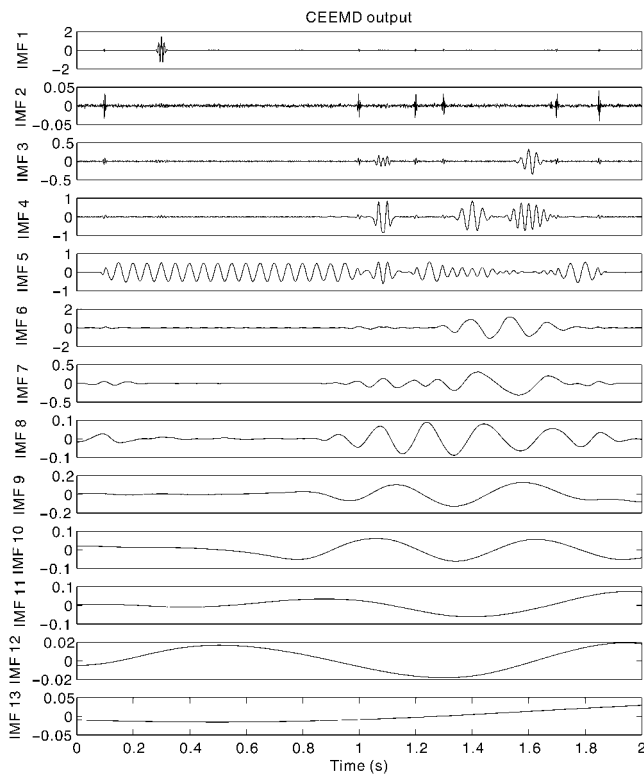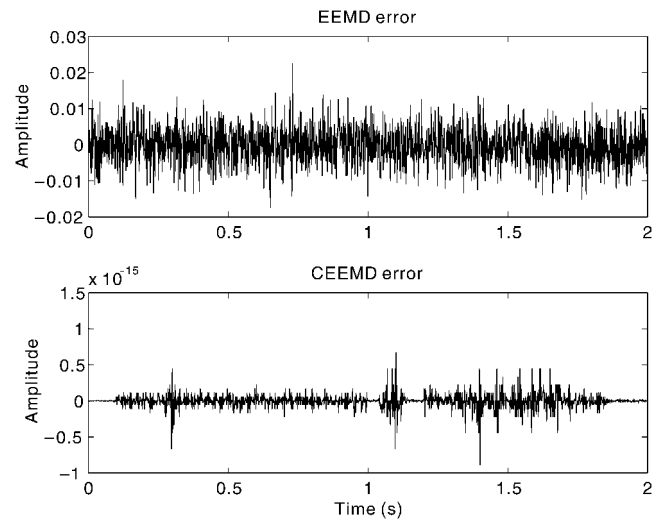

Figure 4. CEEMD output with 10% added Gaussian white noise and 100 realizations. The output is least affected by mode mixing of all EMD variants (compare with Figures 2 and 3).
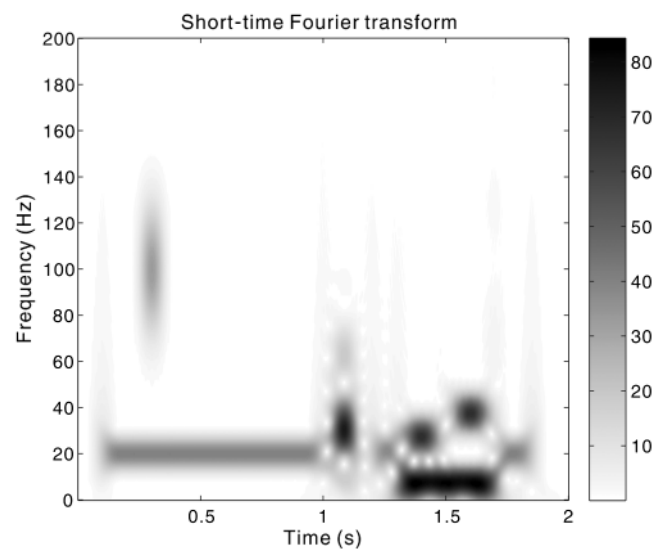

Figure 6. STFT with a 170 ms time window. It cannot distinguish between the two Ricker wavelets at 1.07 and 1.1 s due to its fixed time-frequency resolution.

An erosional surface is located between CMPs 35 and 50 around 0.4 s. The data also contain evidence of migration artifacts (smiles) at the left edge between 0.1 s and 0.6 s. Note that van der Baan et al. (2010) have used cumulative energy and local phase attributes to interpret the same data.

First, we take the trace for CMP 81 (Figure 11) as an example to show the time-frequency distributions corresponding to the various transforms. The results for the short-time Fourier transform with a 50 ms time window and the wavelet transform are shown in Figures 12 and 13, respectively. Both tools show that there are
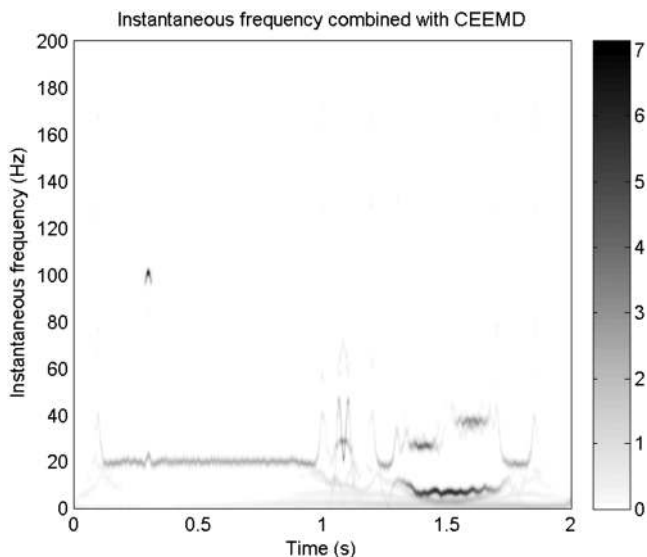
essentially two frequency bands, a lower one between 10 and 50 Hz persistent at all times, and an upper one that diminishes over time (90 Hz at 0.1 s, 70 Hz at 0.5 s, and 50 Hz at 1 s). The reduction in the high-frequency band is most likely due to attenuation of the seismic wavelet.

Instantaneous spectral analysis combined with CEEMD with 10% added Gaussian white noise using 50 realizations (Figure 14) provides a much sparser image. It reflects a similar time-frequency distribution as the two traditional tools with the persistent lower frequency band as well as the diminishing upper band visible. The sparser image is helpful for more accurately locating these spectral anomalies, and thus facilitating further interpretation.

Next, we pick the peak frequency at each time sample and overlay it onto the original seismic data. Figure 15 shows the peak frequency after short-time Fourier transform. This image shows smooth and continuous features, including alternately high- and low-frequency bands between 0.2 and 0.8 s due to variations in reflector spacing, and a general decrease in high frequencies, which is associated with attenuation of the seismic wavelet.

Figure 15 delineates several interesting features in this data set. First, the peak frequency attribute highlights the Cretaceous meandering channels at 0.42 s, which are characterized by lower frequency content due to their increased thickness. Second, it indicates the weakening of the closely spaced reflections (thin layers) around 0.8 s. High peak frequencies are clearly visible between CMPs 0 and 75, followed by predominantly low frequencies due to the thick homogeneous layer underneath. A comparison with the original section (Figure 10) shows indeed a reduction in the number of closely spaced reflections from the left to the right around 0.8 s, although the migration artifacts visible at the left edge may also influence the high-frequency region to some extent.

As first glance, the CEEMD-based peak frequencies seem to be noisier (Figure 16). However, the image contains more fine detail compared with the short-time Fourier result (Figure 15). Both images delineate the Cretaceous meandering channels around 0.42 s. Also, the thin-layer reflection at 0.80 s is more clearly fol-
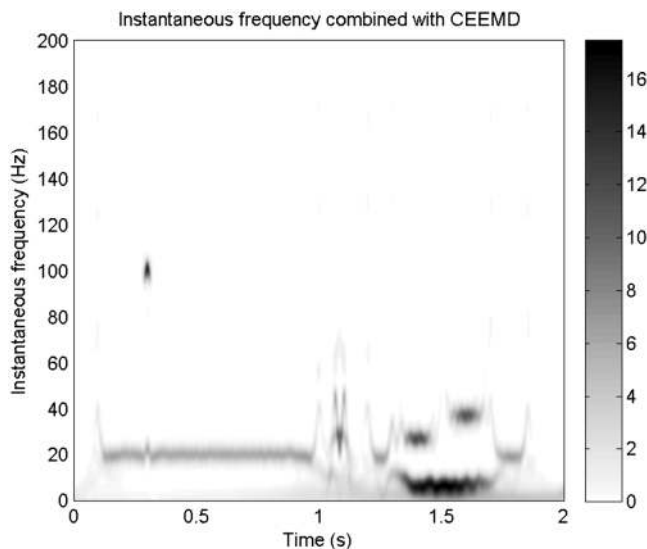

Figure 7. Wavelet transform analysis, which shows a better compromise between time and frequency resolution than the short-time Fourier transform as it distinguishes both Ricker wavelets at 1.1 s. Yet, the frequency resolution for the 100 Hz Morlet wavelet at 0.3 s is poor.

Figure 8. Instantaneous spectrum after CEEMD has the highest time-frequency resolution and identifies all individual components. A 6×6 Gaussian weighted filter is applied for display purposes.

Figure 9. Instantaneous spectrum after CEEMD and a 30×30 Gaussian-weighted filter to make the result more comparable to Figures 6 and 7.

lowed without the abrupt transition to a low-frequency layer at CMP 75 due to the influence of the underlying thick opaque layer. This is a direct result of the higher time resolution of CEEMD combined with computation of instantaneous frequencies. On the other hand, initial inspection of the smoother results for the short-time Fourier transform facilitates interpretation of the CEEMD results.

Next, we extract the 30 and 50 Hz frequency slices after CEEMD and short-time Fourier transforms (Figure 17) to illustrate the higher time-frequency resolution of the CEEMD-based results. The instantaneous spectrum shows much sparser outputs and resolves the spectral characteristics of the various reflections more clearly than the short-time Fourier results. This also explains why the Fourier-based peak-frequency attribute is more continuous than the CEEMD-based result in Figures 15 and 16.

We finally perform a spectral decomposition of a 3D seismic data volume using both approaches. Figure 18 shows a time slice at 420 ms displaying the channel feature as well as a subtle fault. CEEMD again employs 10% added Gaussian white noise and 50 realizations. A window length of 150 ms (75 points) is used for the short-time Fourier transform, producing a frequency step of 7 Hz in the spectral decomposition.

Figure 19a and 19c shows, respectively, the 10- and 30-Hz spectral slices for the instantaneous spectrum after CEEMD at 420 ms. The channel and fault are visible, especially at 30 Hz. Both spectral slices show similar features; yet there are also clear differences, in particular in the amplitudes of the channel, indicating little

Figure 10. Seismic data set from a sedimentary basin in Canada. The erosional surface and channels are highlighted by arrows.

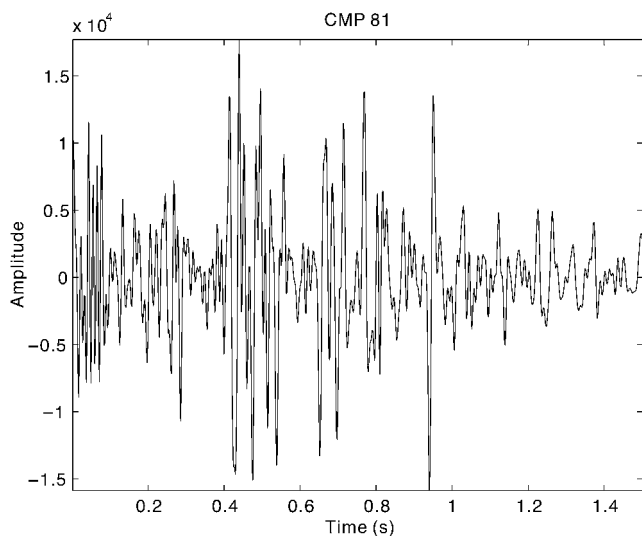Figure 11. Individual trace of CMP 81 in Figure 10. It crossed the channel at 0.42 s.
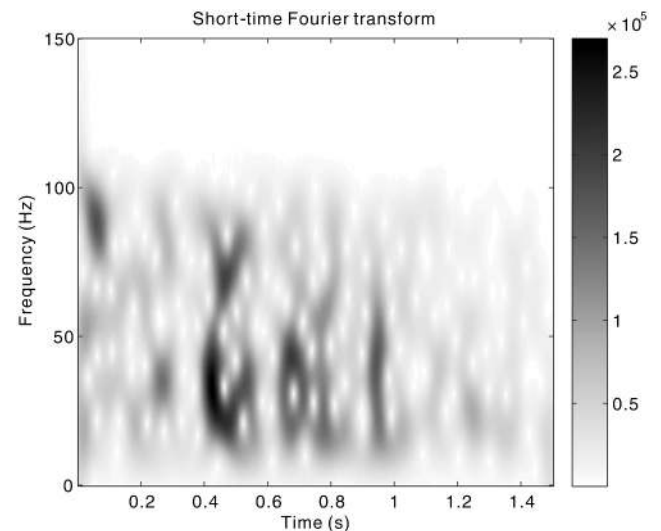

Figure 12. Short-time Fourier transform with a 50 ms time window on CMP 81. The strong 35 Hz anomaly at 0.42 s is due to the channel.
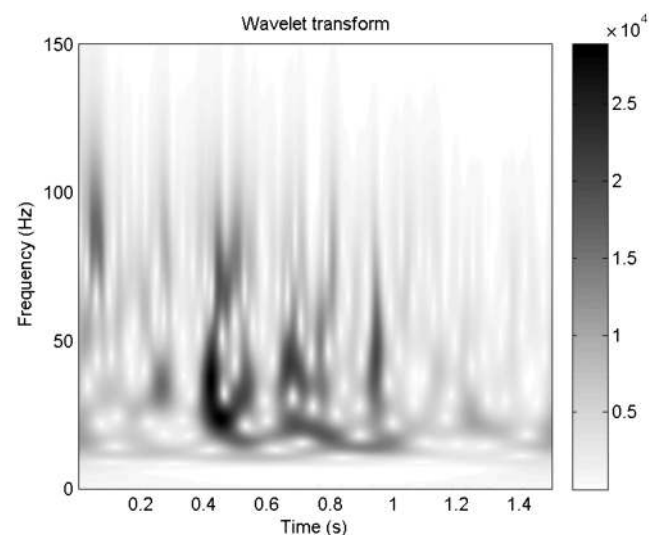

Figure 13. Wavelet analysis on CMP 81. Vertical stripes at higher frequencies are due to an increased time resolution but poorer frequency resolution. High-frequency content is diminishing over time.

spectral leakage across these two frequencies. These amplitude differences are helpful in interpreting thickness variations.

The 10- and 30-Hz spectral slices produced by Fourier analysis also show the fault and channel features (Figure 19b and 19d). However, there are significantly less amplitude variations across both slices as unique frequencies are spaced 7 Hz apart due to the short window length and the spectral leakage inherent to the Fourier transform. This renders interpretation of thickness variations in the channel much more challenging as thinning or thickening by a factor of two may still produce the same amplitudes across several spectral slices centered on the expected peak frequency. We

could have opted for a longer Fourier analysis window, thereby reducing the frequency step in the amplitude spectra. On the other hand, this increases the risk of neighboring reflections negatively biasing the decomposition results. No local analysis window is defined for the CEEMD method, thus circumventing this trade off.

DISCUSSION

Instantaneous frequency can be used to detect and map meandering channels and to determine their thickness (Liu and Marfurt, 2006) as it maps at what frequency maximum constructive interference occurs between the top and bottom channel reflection. However, direct calculation can lead to instantaneous frequencies, which fluctuate rapidly with spatial and temporal location (Barnes, 2007; Han and van der Baan, 2011).

Saha (1987) discusses the relationship between instantaneous frequency and Fourier frequency, and points out that the instantaneous frequency measured at an envelope peak approximates the average Fourier spectral frequency weighted by the amplitude spectrum. Huang et al. (2009) summarize the applicability conditions for instantaneous frequency; namely, the time series must be monocomponent and narrow-band. Analysis of instantaneous frequencies has been gradually replaced by spectral decomposition techniques in the 1990s due to their increased flexibility (Chakraborty and Okaya, 1995; Partyka et al., 1999).

CEEMD successfully overcomes the mode-mixing problem, thus facilitating the analysis of individual IMFs. The subsequent computation of the instantaneous frequency then leads to relatively smoothly varying and positive instantaneous frequencies suitable for time-frequency analysis. In addition, the synthetic and real data examples show this produces a potentially higher time-frequency resolution than the short-time Fourier and wavelet transforms. Window length, overlap, and mother wavelet parameters restrict the resolution of short-time Fourier and wavelet transforms, and predefined decomposition bases render these two methods less suitable for analyzing nonstationary systems.
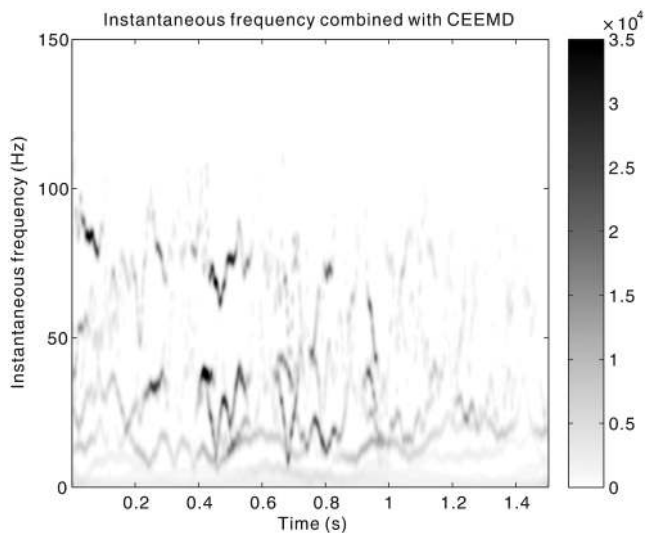

Figure 14. Instantaneous spectrum after CEEMD on CMP 81, displaying the highest time-frequency resolution. Similar features are visible as in Figures 12 and 13 including the channel at 0.42 s and the diminishing high-frequency content over time.
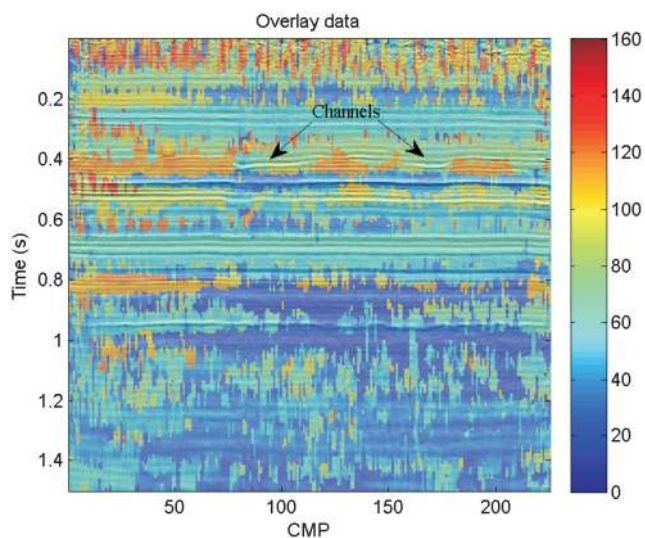

Figure 15. Peak frequency attribute after short-time Fourier transform. The image highlights variations in reflector spacing, laterally (channels) and vertically, as well as the gradually decreasing frequency content with depth due to attenuation.
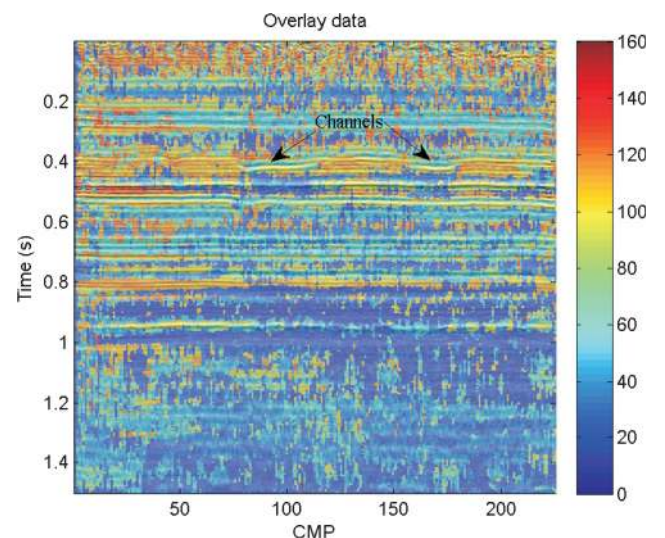

Figure 16. Peak frequency attribute from the instantaneous spectrum and CEEMD. A higher time-frequency resolution leads to more spatial and temporal variations but also a sharper delineation of the channels and individual reflection sequences.

The computational cost of CEEMD is proportional to the number of realizations. We use 50 realizations in the real data application to balance computational cost versus satisfactory decomposition results. Broadly speaking, we found in our tests that the computational cost of a wavelet transform and CEEMD using 50 realizations are, respectively, twice and 18 times that of a short-time Fourier transform. A single EMD decomposition can thus be faster than a single short-time Fourier transform result. Obviously, these computation times strongly depend on the implementation and actual parameter settings, yet applications of EMD and variants are not prohibitively expensive. The actual time-frequency resolution of any EMD variant in combination with computation of the instantaneous frequency is, to the best of our knowledge, still unknown. The uncertainty principle states that it is impossible to achieve simultaneously high time and frequency resolution, as their product is always greater than or equal to a constant. In the short-time Fourier transform, the window length causes the tradeoff between time and frequency resolution. Large time windows achieve good frequency resolution at the cost of high time resolution, and vice versa. Conversely wavelet and S-transforms display an inherent trade-off between time and frequency resolution via their variable-size analysis windows ([Rioul and Vetterli, 1991](#); [Kumar and Foufoula-Georgiou, 1997](#)).

The instantaneous frequency calculates a frequency value at every time sample, producing the highest possible time resolution but with necessarily very poor frequency resolution. This provides an alternative insight into why negative frequency values are not uncommon. However, instantaneous frequency is not meaningless as the instantaneous frequency measured at an envelope peak approximates the weighted average Fourier spectral frequency, and shows superior results on monocomponent and narrow band signals ([Saha, 1987](#); [Huang et al., 2009](#)).

[Flandrin et al. (2004)](#) show that EMD acts as a constant-Q band-pass filter for white-noise time series. In other words, white noise is divided into IMF components, each comprising approximately a single octave. Results by [Torres et al. (2011)](#) imply that CEEMD maintains this property. Given the uncertainty principle, we postulate therefore that the inherent frequency resolution of each individual IMF is one octave with a time resolution inversely proportional to the center frequency of this octave. The obtained IMFs thus have an increasing frequency resolution at the expense of a decreasing time resolution with increasing IMF number. In other words, the first IMF has thus the highest time resolution and the lowest frequency resolution. The opposite is true for the last IMF. This furthermore implies that temporal fluctuations in the instantaneous frequencies are limited to approximately the reciprocal of the center frequency of the corresponding octave, or to put it differently, all computed instantaneous frequencies are guaranteed to be relatively smooth within their various scale lengths.

The preceding discussion assumes a white-noise signal. For arbitrary signals, the performance of CEEMD in combination with

instantaneous attributes may retrieve even more accurate and precise time-frequency decompositions if the original trace is comprised of individual monocomponent and narrowband signals as the sifting algorithm is designed to extract individual IMFs with precisely such characteristics. One important assumption in EMD and its variants is that the observed signal is comprised of narrowband subsignals. The instantaneous frequency of each IMF then accurately captures their characteristics. On the other hand, if
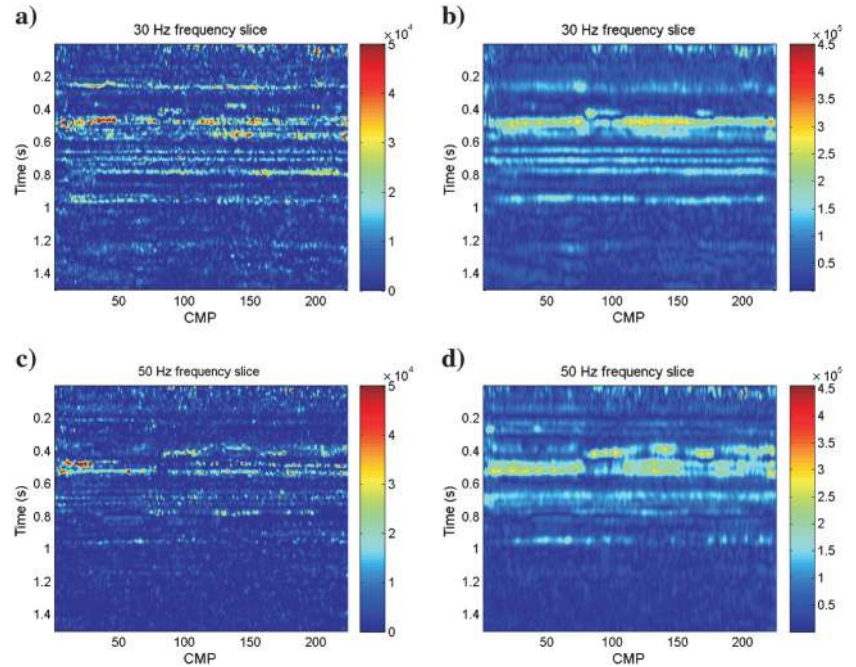

Figure 17. Constant-frequency slices. (a) 30-Hz CEEMD-based method, (b) 30 Hz short-time Fourier transform, (c) 50-Hz CEEMD-based method, (d) 50-Hz short-time Fourier transfrom. The instantaneous spectrum combined with CEEMD shows higher time-frequency resolution than the short-time Fourier transform.
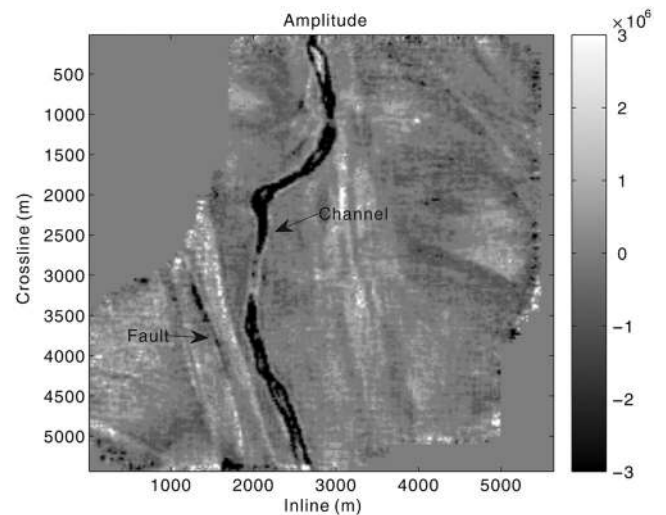

Figure 18. The conventional amplitude slice at time 420 ms. The channel feature is clearly shown.

subsignals have some bandwidth, such as a Ricker wavelet or Morlet wavelet, the described method will seek to collapse this to a single frequency. This could be interpreted as superresolution as it may help in analyzing subtle variations but simultaneously it may hide the true bandwidth of this subsignal. In addition, this may not be suitable for all signal analysis, e.g., if an attenuation analysis is required using spectral ratios (Reine et al., 2009, 2012a, 2012b).

Finally, the main advantages of CEEMD combined with instantaneous frequencies are the ease of implementary and controllable time-frequency resolution. There are only two parameters in CEEMD, namely the percentage of Gaussian white noise and the number of noise-realizations.

Neither seems to have a critical influence on final decompositions. Furthermore, we can control the time-frequency resolution by the size of the Gaussian weighted filter. Smaller sizes show higher temporal-spectral resolution, and vice versa. It is therefore possible to compute first a decomposition result similar to those of the short-time Fourier and wavelet transforms which can then be reduced for further and more precise analysis, thus allowing for seismic interpretation with controllable time-frequency resolution. The real data example verifies that instantaneous spectrum after CEEMD have higher time-frequency resolution than traditional decompositions. However, the associated peak-frequency attribute may therefore vary more rapidly, spatially and temporally, rendering the interpretation more challenging. Our recommendation is to analyze the principal frequency variations by short-time Fourier transform or severely smoothed CEEMD-based instantaneous frequencies first, followed by identification of the subtle changes in geology using the unsmoothed instantaneous spectrum.

CONCLUSION

CEEMD is a robust extension of EMD methods. It solves not only the mode mixing problem, but also leads to complete signal reconstructions. After CEEMD, instantaneous frequency spectra manifest visibly higher time-frequency resolution than short-time Fourier and wavelet transforms on synthetic and field data examples. These characteristics render the technique highly promising for seismic processing and interpretation.

ACKNOWLEDGMENTS

REFERENCES

Barnes, A. E., 2000, Weighted average seismic attributes: Geophysics, **65**, 275–285, doi: 10.1190/1.1444718.
Barnes, A. E., 2007, A tutorial on complex seismic trace analysis: Geophysics, **72**, no. 6, W33–W43, doi: 10.1190/1.2785048.
Battista, B. M., C. Knapp, T. McGee, and V. Goebel, 2007, Application of the empirical mode decomposition and Hilbert-Huang transform to seismic reflection data: Geophysics, **72**, no. 2, H29–H37, doi: 10.1190/1.2437700.
Bekara, M., and M. Van der Baan, 2009, Random and coherent noise attenuation by empirical mode decomposition: Geophysics, **74**, no. 5, V89–V98, doi: 10.1190/1.3157244.
Boashash, B., and M. Mesbah, 2004, Signal enhancement by time-frequency peak filtering: IEEE Transactions on Signal Processing, **52**, 929–937, doi: 10.1109/TSP.2004.823510.
Castagna, J., S. Sun, and R. Siegfried, 2003, Instantaneous spectral analysis: Detection of low-frequency shadows associated with hydrocarbons: The Leading Edge, **22**, 120–127, doi: 10.1190/1.1559038.
Chakraborty, A., and D. Okaya, 1995, Frequency-time decomposition of seismic data using wavelet-based methods: Geophysics, **60**, 1906–1916, doi: 10.1190/1.1443922.
Deering, R., and J. F. Kaiser, 2005, The use of a masking signal to improve empirical mode decomposition, in acoustics, speech, and signal processing, 2005: Proceedings of the IEEE International Conference, IV485–IV488.
Flandrin, P., G. Rilling, and P. Goncalves, 2004, Empirical mode decomposition as a filter bank: IEEE Signal Processing Letters, **11**, 112–114, doi: 10.1109/LSP.2003.821662.
Fomel, S., 2007, Local seismic attributes: Geophysics, **72**, no. 3, A29–A33, doi: 10.1190/1.2437573.
Han, J., and M. Van der Baan, 2011, Empirical mode decomposition and robust seismic attribute analysis: CSPG CSEG CWLS Convention, **114**.
Huang, J., and B. Milkereit, 2009, Empirical mode decomposition based instantaneous spectral analysis and its applications to heterogeneous petrophysical model construction: CSPG CSEG CWLS Convention, 205–210.
Huang, N. E., 1999, A new view of nonlinear water waves: The Hilbert spectrum: Annual Review of Fluid Mechanics, **31**, 417–457, doi: 10.1146/annurev.fluid.31.1.417.
Huang, N. E., Z. Shen, S. R. Long, M. C. Wu, H. H. Shih, Q. Zheng, N.-C. Yen, C. C. Tung, and H. H. Liu, 1998, The empirical mode decomposition and the Hilbert spectrum for nonlinear and non-stationary time series analysis: Proceedings of the Royal Society of London, Series A: Mathematical, Physical and Engineering Sciences, **454**, no. 1971, 903–995, doi: 10.1098/rspa.1998.0193.
Huang, N. E., M.-L. C. Wu, S. R. Long, S. S. P. Shen, W. Qu, P. Gloersen, and K. L. Fan, 2003,
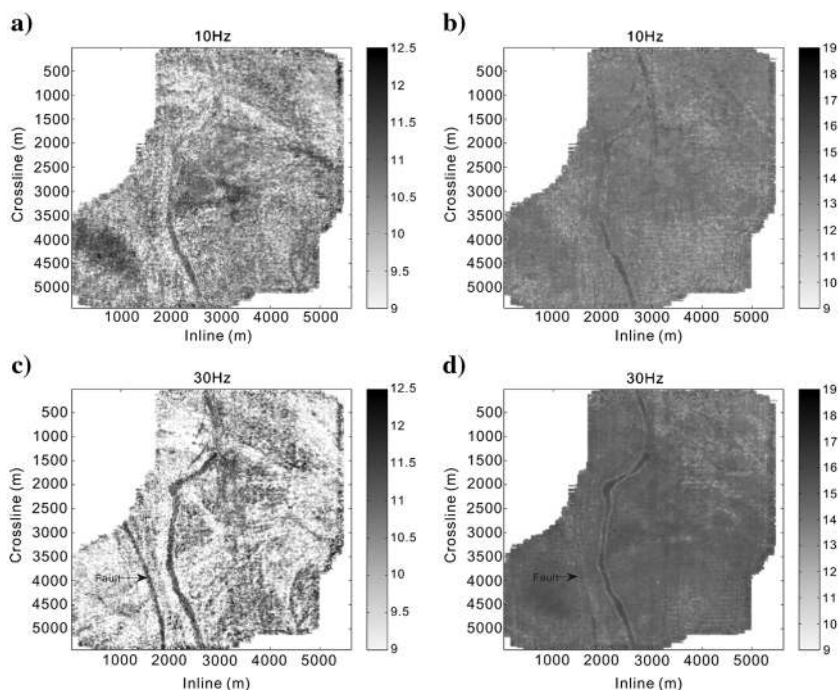

Figure 19. Comparison of time slices: (a) 10 Hz of CEEMD-based method; (b) 10 Hz of short-time Fourier transform; (c) 30 Hz of CEEMD-based method; (d) 30 Hz of short-time Fourier transform. CEEMD-based method highlights the geologic features more clearly and facilitates the interpretation of thickness variation.

A confidence limit for the empirical mode decomposition and Hilbert spectral analysis: Proceedings of the Royal Society of London. Series A, Mathematical and Physical Science, 2037, 2317–2345, doi: 10.1098/rspa.2003.1123.

Huang, N. E., and Z. Wu, 2008, A review on Hilbert-Huang transform: Method and its applications to geophysical studies: Reviews of Geophysics, **46**, no. 2, RG2006, doi: 10.1029/2007RG000228.

Huang, N. E., Z. Wu, S. R. Long, K. C. Arnold, X. Chen, and B. Karin, 2009, On instantaneous frequency: Advances in Adaptive Data Analysis, **1**, no. 2, 177–229, doi: 10.1142/S1793536909000096.

Kumar, P., and E. Foufoula-Georgiou, 1997, Wavelet analysis for geophysical applications: Reviews of Geophysics, no. 4, 385–412, doi: 10.1029/97RG00427.

Li, Y., and X. Zheng, 2008, Spectral decomposition using Wigner-Ville distribution with applications to carbonate reservoir characterization: The Leading Edge, **27**, 1050–1057, doi: 10.1190/1.2967559.

Liu, G., S. Fomel, and X. Chen, 2011, Time-frequency analysis of seismic data using local attributes: Geophysics, **76**, no. 6, P23–P34, doi: 10.1190/geo2010-0185.1.

Liu, J., and K. J. Marfurt, 2006, Thin bed thickness prediction using peak instantaneous frequency: 76th Annual International Meeting, SEG, Expanded Abstracts, 968–972.

Liu, J., and K. J. Marfurt, 2007, Instantaneous spectral attributes to detect channels: Geophysics, **72**, no. 2, P23–P31, doi: 10.1190/1.2428268.

Magrin-Chagnolleau, I., and R. G. Baraniuk, 1999, Empirical mode decomposition based time-frequency attributes: 69th Annual International Meeting, SEG, 1–4.

Mallat, S., 2008, A wavelet tour of signal processing: The sparse way: Academic Press, 98–99.

Marfurt, K. J., and R. L. Kirlin, 2001, Narrow-band spectral analysis and thin-bed tuning: Geophysics, **66**, 1274–1283, doi: 10.1190/1.1487075.

Morlet, J., G. Arensz, and E. Fourgeau, 1982, Wave propagation and sampling theory-part II: Sampling theory and complex waves: Geophysics, **47**, 222–236, doi: 10.1190/1.1441329.

Odebeatu, E., J. Zhang, M. Chapman, E. Liu, and X. Y. Li, 2006, Application of spectral decomposition to detection of dispersion anomalies associated with gas saturation: The Leading Edge, **25**, 206–210, doi: 10.1190/1.2172314.

Partyka, G., J. Gridley, and J. Lopez, 1999, Interpretational applications of spectral decomposition in reservoir characterization: The Leading Edge, **18**, 353–360, doi: 10.1190/1.1438295.

Reine, C., R. Clark, and M. Van der Baan, 2012a, Robust prestack Q-determination using surface seismic data: I — Method and synthetic examples: Geophysics, **77**, no. 1, R45–R56, doi: 10.1190/geo2011-0073.1.

Reine, C., R. Clark, and M. Van der Baan, 2012b, Robust prestack Q-determination using surface seismic data: II — 3Dcase study: Geophysics, **77**, no. 1, B1–B10, doi: 10.1190/geo2011-0074.1.

Reine, C., M. Van der Baan, and R. Clark, 2009, The robustness of seismic attenuation measurements using fixed- and variable-window time-frequency transforms: Geophysics, **74**, no. 2, WA123–WA135, doi: 10.1190/1.3043726.

Rioul, O., and M. Vetterli, 1991, Wavelets and signal processing: IEEE Signal Processing Magazine, **8**, 14–38, doi: 10.1109/79.91217.

Saha, J. G., 1987, Relationship between fourier and instantaneous frequency: 57th Annual International Meeting, SEG, Expanded Abstracts, 591–594.

Stockwell, R. G., L. Mansinha, and R. P. Lowe, 1996, Localization of the complex spectrum: The S-transform: IEEE Transactions on Signal Processing, **44**, 998–1001, doi: 10.1109/78.492555.

Taner, M. T., F. Koehler, and R. E. Sheriff, 1979, Complex seismic trace analysis: Geophysics, **44**, 1041–1063, doi: 10.1190/1.1440994.

Torres, M. E., M. A. Colominas, G. Schlotthauer, and P. Flandrin, 2011, A complete ensemble empirical mode decomposition with adaptive noise: IEEE International Conference on Acoustics, Speech and Signal Processing (ICASSP), 4144–4147.

Van der Baan, M., S. Fomel, and M. Perz, 2010, Nonstationary phase estimation: A tool for seismic interpretation?: The Leading Edge, **29**, 1020–1026, doi: 10.1190/1.3485762.

Wu, Z., and N. E. Huang, 2009, Ensemble empirical mode decomposition: A noise-assisted data analysis method: Advances in Adaptive Data Analysis, **01**, no. 01, 1–41, doi: 10.1142/S1793536909000047.